ROYAL SOCIETY OF CHEMISTRY

CrossMark
click for updates

Three-dimensional hierarchical cultivation of human skin cells on bio-adaptive hybrid fibers†

Viktoria Planz,‡[a] Salem Seif,‡[ab] Jennifer S. Atchison,[c] Branko Vukosavljevic,[d] Lisa Sparenberg,[a] Elmar Kroner[c] and Maike Windbergs*[abd]

The human skin comprises a complex multi-scale layered structure with hierarchical organization of different cells within the extracellular matrix (ECM). This supportive fiber-reinforced structure provides a dynamically changing microenvironment with specific topographical, mechanical and biochemical cell recognition sites to facilitate cell attachment and proliferation. Current advances in developing artificial matrices for cultivation of human cells concentrate on surface functionalizing of biocompatible materials with different biomolecules like growth factors to enhance cell attachment. However, an often neglected aspect for efficient modulation of cell–matrix interactions is posed by the mechanical characteristics of such artificial matrices. To address this issue, we fabricated biocompatible hybrid fibers simulating the complex biomechanical characteristics of native ECM in human skin. Subsequently, we analyzed interactions of such fibers with human skin cells focusing on the identification of key fiber characteristics for optimized cell–matrix interactions. We successfully identified the mediating effect of bio-adaptive elasto-plastic stiffness paired with hydrophilic surface properties as key factors for cell attachment and proliferation, thus elucidating the synergistic role of these parameters to induce cellular responses. Co-cultivation of fibroblasts and keratinocytes on such fiber mats representing the specific cells in dermis and epidermis resulted in a hierarchical organization of dermal and epidermal tissue layers. In addition, terminal differentiation of keratinocytes at the air interface was observed. These findings provide valuable new insights into cell behaviour in three-dimensional structures and cell–material interactions which can be used for rational development of bio-inspired functional materials for advanced biomedical applications.

1. Introduction

In-depth understanding of the composition of human tissues and interactions of their individual components currently attracts profound interest for elucidating natural processes as well as for developing bio-inspired functional materials.[1,2] In the biomedical context, one unique natural structure is represented by the extracellular matrix (ECM), which forms the basic framework for all tissues in the human body. Based on a fibrillar network,

the ECM provides three-dimensional structural support for adherence as well as for cell infiltration during migration and differentiation processes.[3] Depending on the tissue, different cell types co-exist within the ECM in a specific hierarchical order. Thus, an artificial imitation of native ECM is highly interesting with the potential to address basic research questions like cell behavior in three-dimensional structures as well as cell–material interactions with a perspective for bio-inspired products like wound dressings.[4–8]

In this context, physicochemical material characteristics like wettability and surface roughness which affect cell attachment and proliferation have extensively been investigated.[9–11] However, only recently the high importance of biomechanical properties within hierarchical native biostructures was discovered.[12–14]

In human ECM, collagen and elastin fibers as the main constituents exhibit a complex interplay upon mechanical forces.[15–17] Elastin fibers act as energy absorbers resulting in fiber fracture, while the consecutive load transfer to the larger collagen fibers leads to realignment and significant fiber elongation. Exceeding the critical yield stress causes plastic deformation of the collagen fibers by separation into fiber substructures prior

a Department of Biopharmaceutics and Pharmaceutical Technology, Saarland University, Campus Building A 4.1, 66123 Saarbrücken, Germany. E-mail: m.windbergs@mx.uni-saarland.de; Fax: +49 681 98806 1009; Tel: +49 681 98806 1040
b PharmBioTec GmbH, Science Park 1, 66123 Saarbrücken, Germany
c INM – Leibniz Institute for New Materials, Campus Building D 2.2, 66123 Saarbrücken, Germany
d Helmholtz Centre for Infection Research (HZI) and Helmholtz Institute for Pharmaceutical Research Saarland (HIPS), Department of Drug Delivery (DDEL), Campus Building E 8.1, 66123 Saarbrücken, Germany
† Electronic supplementary information (ESI) available. See DOI: 10.1039/c6ib00080k
‡ Authors contributed equally to the manuscript.

to failure.[18,19] Computational-based simulations of the hierarchical architecture of collagen could successfully demonstrate this mechano-mutable behavior at multi-scale level upon controlled mechanical stress.[20–22]

The aim of this study was to transfer this recent knowledge for fabricating biocompatible fibers by electrospinning which simulate the complex biomechanical characteristics of native ECM in human skin. Hybrid fibers based on biocompatible materials were fabricated with the intention to mimic the synchronized interplay of adequate substrate stiffness and flexibility found in ECM as a prerequisite for favored cell–material interactions. Further, advanced biomechanical testing and interaction studies with primary human skin cells were performed with the newly designed fibers to identify key characteristics for cell attachment and proliferation.

2. Materials and methods

2.1 Fabrication of electrospun scaffolds

Fiber mats were prepared by pumping a polycaprolactone (PCL) solution (12% w/v in chloroform/ethanol 1:1, molecular weight 80 000, Sigma-Aldrich, Steinheim, Germany) through a syringe nozzle using a flow rate of 3 ml h^{-1} and applying voltage of 8 kV. The formed fibers were deposited on a drum collector rotating at a speed of 0.5 m s^{-1} with a nozzle to collector distance of 13 cm. Blend fiber mats were fabricated based on the PCL/gelatin mixture (3:1 w/w, gelatin type A, 300 Bloom, Sigma-Aldrich, Steinheim, Germany) in 2,2,2-trifluoroethanol (TFE) (purity $\geq$ 99%, Sigma-Aldrich, Steinheim, Germany) at a concentration of 9% (w/v). The pumping flow rate was 3 ml h^{-1}, while the voltage was 7 kV. The syringe nozzle was located 17 cm from a drum collector rotating at 0.5 m s^{-1}. For hybrid fiber mats, two polymeric solutions were simultaneously spun allowing two types of fibers to form one fiber mat. For gelatin fibers, a flow rate of 2 ml h^{-1}, high voltage of 14 kV, and a nozzle to collector distance of 15 cm were applied. For blend fibers, a pumping flow rate of 1.5 ml h^{-1}, high voltage of 8 kV, and a nozzle to collector distance of 17 cm were used. Both fibers were simultaneously collected on the same drum collector rotating at a speed of 0.5 m s^{-1} to assure homogeneous distribution of the fibers within the fiber mat.

2.2 Confocal Raman microscopy

Confocal Raman microscopy (CRM, WITec alpha 300R+; WITec GmbH, Ulm, Germany) was utilized for chemical imaging to characterize the distribution of PCL and gelatin within the electrospun fibers. The setup was equipped with a Zeiss Epiplan Neofluar objective (50$\times$/NA = 0.8 or 100$\times$/NA = 0.9). Images were recorded using a diode laser with an excitation wavelength of 532 nm adjusted to a power of 20 mW before the objective. Raman spectra were acquired with a spatial resolution of 0.25 μm. Data processing and analysis were performed using WITec Project Plus software (WITec GmbH, Ulm, Germany). After removal of cosmic ray peaks and background subtraction, the collected Raman spectra were converted into false color images by supervised cluster analysis.

2.3 Physicochemical characterization of the electrospun scaffolds

Visualization of the morphological appearance of the electrospun fibers was carried out by scanning electron microscopy (SEM) using a Zeiss EVO HD 15 (Carl Zeiss AG, Oberkochen, Germany) at an acceleration voltage of 5 kV. The specimen preparation for SEM imaging included the coating of the sample surface with a thin gold layer using the sputter coater Quorum Q150R ES (Quorum Technologies Ltd, East Grinstead, UK). For the determination of the average diameter of the fibers and the pore sizes, randomly selected fibers were measured based on SEM images using ImageJ software (National Institutes of Health, USA).

Wetting properties of the electrospun fiber mats were evaluated by contact angle measurements calculating the slope of the tangent to the drop at the liquid–solid interface. Droplets with a volume of 1 μl were dispensed onto the scaffolds using a Hamilton syringe. After 5 s of incubation, the contact angle was acquired with a camera based measurement device CAM 100 (KSV Instruments Ltd, Helsinki, Finland).

Determination of the fiber mat thickness on randomly selected sample punches of the fiber mats was performed with a surface testing instrument MiniTest 3100 (ElektroPhysik Dr Steingroever GmbH & Co. KG, Cologne, Germany) based on magnetic induction. Mechanical properties of the fiber mats were determined by using a table top material testing machine from Inspekt Table Blue (Hegewald & Peschke, Nossen, Germany) by loading tension with a 5 kN load cell under constant cross head speed of 5 mm min^{-1}. Fiber mat samples were cut into rectangles of 4 $\times$ 1 cm and mounted into paper frames with an opening of 3 $\times$ 1 cm. Before applying tension, the frames were clamped with grips and cut on both lateral sides to allow for consistent loading of the samples, thus initiating the tensile test in a reproducible manner. The Young's modulus was determined by calculating the slope of the initial linear elastic region of the stress–strain curve.

2.4 Human skin preparation

Human skin was immediately received after excision from plastic surgery of female Caucasians (Department of Plastic and Hand Surgery, Caritas-Krankenhaus, Lebach, Germany) based on an ethical approval of the Saarland ethics commission (no. 88/12) and informed consent of the donors. For further proceeding, removal of the subcutaneous fat layer was performed by a scalpel and the remaining tissue was stored at -26 °C.

2.5 Extracellular matrix isolation

The isolation of native extracellular matrix based on excised human skin included two process steps. First, the deepidermization of the skin specimens was performed by heat separation. In detail, skin biopsy punches were incubated in a water bath (60 °C) for 90 s to remove the epidermis by peeling it off from the underlying dermal part using forceps. The deepidermized dermis samples were subsequently immersed in 1 M sodium hydroxide solution and stored at 37 °C for 24 h

under gentle stirring conditions to induce the decellularization of the tissue.

2.6 Degradation study

The degradation kinetics of gelatin from hybrid fiber mats were evaluated by calculating the weight loss. Previous weighed 1.2 cm punches of the hybrid fibers (about 3–4 mg each) were placed in glass vials containing 5 ml phosphate buffer solution (BSA, pH 7.4) and incubated at 37 °C for a defined period of time without shaking. At predetermined intervals, triplicate samples were removed from the test vials and analyzed. After drying at 37 °C for 24 h, the weight loss of the punches was determined in comparison to their initial weight.

2.7 Cultivation of human cells

Human primary dermal fibroblasts (NHDF-p, cat. no. C-12352) were purchased from PromoCell GmbH (Heidelberg, Germany). The immortalized human keratinocyte cell line HaCaT was kindly provided by Prof. N. Fusenig (German Cancer Research Center, Heidelberg, Germany).[23] The cells were cultivated in high-glucose Dulbecco modified Eagle's medium (Gibco® Life Technologies, Darmstadt, Germany) supplemented with 10% fetal bovine serum (Lonza, Verviers, Belgium). The cultures were maintained at 37 °C in a humidified 5% CO_2 atmosphere with medium refreshed every two days.

2.8 Cell cultivation on electrospun scaffolds

For cell cultivation, punches of 1.8 cm in diameter were prepared from PCL, blend and hybrid fiber mats. The punches were placed in 24-well plates (Greiner Bio-One GmbH, Frickenhausen, Germany) covering the whole seeding area of the well to prevent cell attachment to the well bottom. Human dermal fibroblasts were seeded at a density of 0.1×10^6 cells per well by slowly dropping the cell suspension onto the fiber mats and cultivated for 14 days. To resemble the epidermal layer, keratinocytes were seeded on top of the scaffold at a density of 0.1×10^6 cells per well and submersed cultivated for 10 days with further cultivation at air–liquid interface to induce barrier formation for 14 days. The cell-scaffold constructs were cultivated in Dulbecco modified Eagle's medium supplemented with 10% fetal bovine serum and 1% penicillin/streptomycin (PAA Laboratories, Pasching, Austria) at 37 °C in a humidified incubator gassed with 5% CO_2. The medium was carefully replaced every two days during a culture period of 38 days.

2.9 Histology

Histological assessment of the cell-scaffold constructs was performed by fixation in 4% buffered formalin, dehydration in ascending concentrations of ethanol followed by xylol incubation before paraffin embedding. Tissue sections were stained with hematoxylin/eosin (Carl Roth GmbH & Co. KG, Karlsruhe, Germany).

2.10 Cell viability

The viability of human dermal fibroblasts cultivated for five days on fiber mats was investigated by determining the amount of lactate dehydrogenase (LDH) released from cells with damaged cell membrane into the surrounding cell culture medium (Cytotoxicity Detection Kit, Roche Diagnostics, Mannheim, Germany). Absorbance values were measured using a plate reader at 550 nm wavelength.

2.11 Fluorescence staining

Evaluation of the cell behavior focusing on cell attachment, migration and proliferation of NHDF-p cells cultured on the different fiber types was performed by staining with Rhodamine labeled *Ricinus Communis Agglutinin I* (Vector Laboratories, CA, USA) to visualize the cell membrane and 4,6-diamidin-2-phenyl-indole (DAPI) obtained from Sigma-Aldrich (Steinheim, Germany) for cell nucleus labeling. Briefly, samples were washed with PBS, fixed in ice cold methanol for 10 minutes at 4 °C and rinsed again with PBS prior to the staining with the fluorescence dyes. Samples were analyzed by Zeiss LSM 700 confocal laser scanning microscopy (Jena, Germany).

2.12 Immunofluorescence staining

Assessment of barrier formation of the reconstructed skin tissue was performed by immunofluorescence staining using mouse monoclonal antibody against involucrin (Abcam ab68, Cambridge, United Kingdom). For antigen retrieval, a gentle antigen unmasking method was used by incubating the slides in 10 mM citrate buffer (pH 6.0) at 37 °C for 30 minutes. Tissue permeabilization and blocking of unspecific binding sites was achieved by using buffered solution of 0.05% saponin and 1% bovine serum albumin for 30 minutes at room temperature before primary antibody incubation at a 1 : 100 dilution overnight at 4 °C in a humidified chamber. Secondary polyclonal rabbit anti-mouse antibody conjugated with Alexa Fluor 488® (A-11059, Life Technologies, Carlsbad, CA, USA) was applied at a 1 : 500 dilution for 1 hour at room temperature. Nuclei counterstaining was performed using DAPI.

3. Results and discussion

3.1 Fabrication and characterization of bio-inspired electrospun fibers

Intensive research has been conducted to analyze the complex interactions of human cells with material surfaces for rational development of functional healthcare materials.[24] As the native ECM exhibits a fibrous structure, numerous studies focused on the analysis of biocompatible fibers and cells elucidating the influence of factors like *e.g.* surface wettability, fiber diameter and roughness.[25–29] However, even though the biomechanics within human tissues have been identified to play a vital role for cell growth, the relationship of biomechanical fiber characteristics and cellular response has not thoroughly been investigated yet.

To address this gap, we designed different types of electrospun fiber mats with individual biomechanical characteristics and analyzed and evaluated their interactions with primary human cells.

As a first approach, we electrospun one component fiber mats based on polycaprolactone (PCL), a FDA-approved, biocompatible polymer, which is insoluble in water providing a mechanically stable and flexible fiber matrix.[30] Further, to increase the wettability of the fiber surface and to coordinate the biomechanical fiber behavior using a multi-component system, we electrospun blend fibers by mixing PCL with gelatin as a natural, water soluble polymer.[31] Electrospinning of scaffolds made of PCL and gelatin has previously been reported using PCL for mechanical strength and gelatin for optimized cell attachment.[32–37] However, adequate cell attachment properties and proliferation capability as well as optimized cell penetration into the scaffold induced by sufficient scaffold porosity are critical aspects, which are still challenging to realize in case of only PCL/gelatin blend fibers. Initial attempts focused on surface modification with cost-intense bio-functionalization using collagen type I to increase the number of adhered cells.[38] Cell seeding from both scaffold sides was addressed to improve the extent of cell penetration into the scaffold.[36] Further, salt leaching procedures of the fibers were considered to increase scaffold porosity.[37] However, all these procedures are either cost-intense or accompanied by an artificial nature. Therefore, we developed as a third approach a novel compositional assembly of PCL and gelatin to fabricate scaffolds designated as "hybrid" fibers. Specifically, combining pure gelatin fibers with blend fibers (PCL/gelatin) into one scaffold based on a novel co-electrospinning setup was intended to attain a dense fiber network for the initial phase of cell attachment with a high proportion of gelatin providing more cell attachment points. Upon degradation of the pure gelatin fibers and out of the blend fibers within the hybrid assembly, the porosity of the fiber mat increases, leaving more space for scaffold infiltration. Hereby, modulation of fiber mechanics was addressed by the combination of two polymers as well as

different diameters of the two fiber types within the hybrid matrix. All three types of fiber mats were compared to native human ECM which was isolated from human skin and subsequently decellularized. Each fiber mat exhibited a homogenous fiber network with well-defined, interconnected porosity similar to the hierarchical architecture of native ECM and smooth surface (Fig. 1A). With respect to fiber diameter, especially the hybrid fibers were closely comparable to native ECM.

As the spatial distribution of different compounds in one fiber strongly affects the biomechanical properties of the material, we visualized the localization of PCL and gelatin in the blend fibers by confocal Raman microscopy as a non-invasive and chemically selective analytical technique. Based on z-stack analysis, virtual slices of the fibers in different focal planes allowed for spatially resolved, three-dimensional visualization of the fiber composition. One representative false-color image is depicted in Fig. 1B. Interestingly, gelatin (green) is mainly found at the surface of the fiber, whereas the cores of the fibers consist of pure PCL (red).

In addition, to exclude any adverse effects of the electrospun fiber mats on human cells, we performed biocompatibility testing by lactate dehydrogenase (LDH) release analysis, an established test for cell viability. Primary human fibroblasts were cultivated on the fiber mats in conventional cell culture multi-well plates for five days. Based on the respective LDH release, cells grown on fiber mats (independent of their composition) showed a higher viability compared to the ones cultivated on standard polystyrene surfaces of culture wells (Fig. 1C).

As the surface wettability is a well-known determinant influencing the biological behavior of cells on material surfaces, contact angle measurements were performed on the individual fiber mats. PCL fibers exhibited a rather hydrophobic surface indicated by a contact angle of 119°, whereas incorporation of
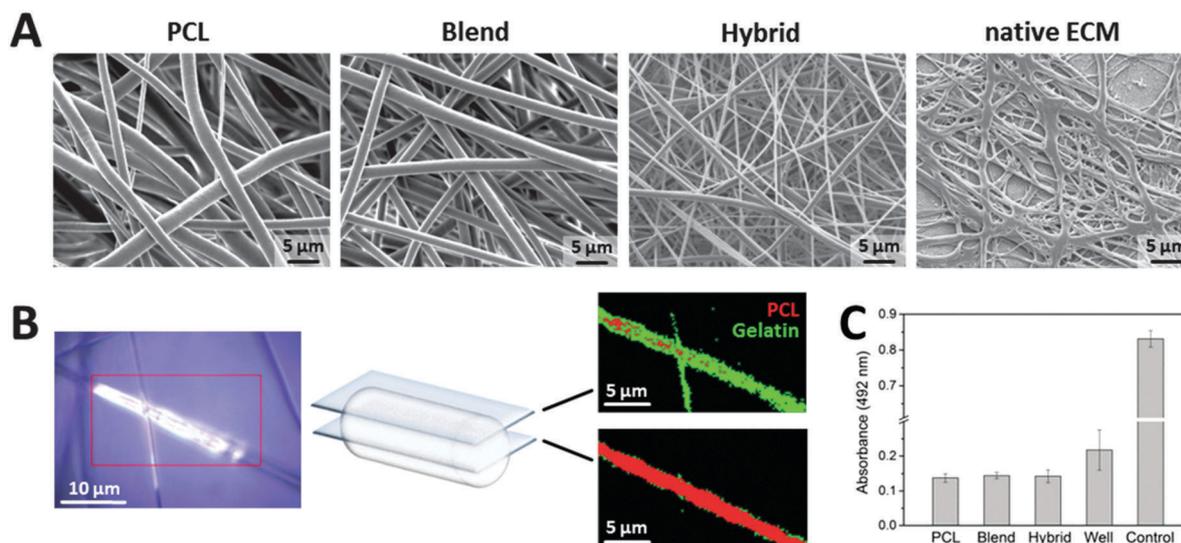

Fig. 1 Characterization of electrospun PCL, blend and hybrid fiber mats. (A) Analysis of fiber morphology based on SEM images. (B) Non-invasive, chemically selective Raman analysis of compound distribution (PCL – red, gelatin – green) in electrospun hybrid fibers. (C) Biocompatibility testing of electrospun fiber mats cultivated for five days with human dermal fibroblasts using the LDH release assay compared to cells cultivated without fiber matrix support in a well. Cells treated with 1% Triton X-100 served as control for cytotoxicity.
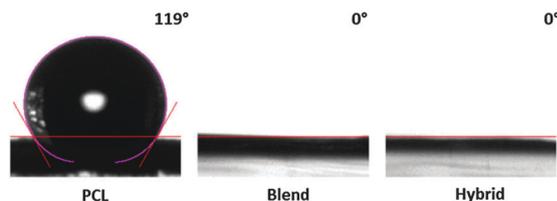
Fig. 2 Evaluation of the wetting properties of electrospun PCL, blend and hybrid fiber mats by contact angle measurements (n = 5).

gelatin as a second component in the blend and hybrid fibers significantly improved the hydrophilicity of the fiber surfaces with contact angles of 0°, thus demonstrating their excellent wettability (Fig. 2).

3.2 Evaluation of mechano-adaptive fiber characteristics

As the main focus of this study, comprehensive biomechanical testing was performed with the fabricated fibers as the biophysical micro-environment plays a crucial role as regulator of cell behavior like migration and proliferation.[39–41]

In this respect, sufficient matrix stiffness is of high importance for anchorage-dependent cells facilitating bonding to the matrix and cell proliferation. In contrast, cell adhesion and proliferation were found to be dramatically reduced upon contact with soft matrices.[40] However, intermediate matrix stiffness was identified as the best promotor for cell motility after successful adherence and proliferation.[40] These findings demonstrate the complexity of biomechanical requirements for optimized cell cultivation with the intention to mimic the native situation. For fibroblasts, Wong et al. reported the capability of these cells to probe substrate rigidity by their filopodia extensions and to adapt their cell response accordingly. They demonstrated the inhibition of focal adhesion maturation and facilitation of cell retraction on soft matrices, whereas rigid substrates promoted cell adhesion and spreading.[42] Therefore, a synchronized interplay of adequate substrate stiffness and flexibility is a prerequisite for favored cell–matrix interactions. Based on the existing knowledge that cell attachment and proliferation are promoted on stiff matrices and cell migration on an intermediate stiffness level, we aimed at introducing both aspects by providing a dynamically changing environment due to gradual gelatin degradation.[39,40] Hereby, the great amount of gelatin at the beginning of cultivation assured high fiber stiffness due to its brittle nature to promote cell attachment and proliferation. Dependent on the rate of gelatin degradation, a successive reduction in fiber stiffness is achieved, thus favoring cell infiltration into the scaffold. Another important parameter is toughness as determinant of the energy amount absorbed by a material prior to fracture. Sufficient toughness of engineered fibers to withstand contractile forces of cells attaching to the fibers is mandatory.[39] However, mimicking the optimal combination of stiffness and toughness of native ECM is a challenging task.[43,44] Based on the recent knowledge from materiomics, we followed two strategic approaches to design fiber mats intending to simulate the biomechanical properties of native ECM.[43,45–47] First, we generated multi-component fibers of different materials (PCL and gelatin) to modulate the

biomechanical behavior of pure PCL fibers. As a second strategy, we fabricated hybrid fiber mats based on the PCL/gelatin blend fibers and additional pure gelatin fibers to combine two types of fibers exhibiting different mechanical characteristics in one fiber mat. We evaluated our fabricated fibers in terms of their stiffness, flexibility and toughness properties by mechanical testing with special focus on elucidating the mechanism of fiber failure. The three different fiber mats (PCL, blend and hybrid) were characterized by uniaxial tensile testing capturing the dynamic structural changes of the fibers and their failure upon tensile loading. The PCL fiber mats started to deform by extensive necking and continuous propagation along the tension axis until the final fiber failure was attained by rapid crack propagation from the edge at a point of weakness. After tensile loading, inter-fiber fusing and negligible fiber alignment could be visualized based on electron microscopy analysis (Fig. 3A). The main reason for the bulk-like failure behavior which is also reflected in the stress–strain curve (Fig. 3B) might be related to the dense fusion of the individual fibers which does not allow for reorientation or unraveling of individual fibers.[43] In comparison, the blend fiber mats exhibited non-uniform elongation properties along the tensile axis. With ongoing deformation, defects started to appear at different positions of the sample until a critical defect density led to failure (Fig. 3A).[46] The fracture process of blend fibers could generally be identified as tearing failure starting from the sample edge with rapid propagation along the sample surface. After tensile loading, electron microscopy revealed less fiber fusing and notable fiber alignment in the direction of the tensile stress (Fig. 3A). This behavior might be related to the core–shell structure of the fibers (shell-gelatin, core-PCL). It is known that gelatin fibers are considerably stiffer than PCL fibers as reflected by the higher Young's modulus of gelatin.[32] Thus, compared to pure PCL fibers, blending PCL with gelatin to form two-component fibers considerably altered their biomechanical characteristics towards a stiffer and tougher matrix as indicated by the steep shift of the linear elastic phase within the stress–strain curve of blend fibers in y-direction (Fig. 3B). In contrast to the rapid crack propagation of PCL and blend fibers, hybrid fibers failed by gradual fiber breakage. Under tensile loading, hybrid fibers exhibited significant reorganization and alignment along the tensile axis during the test. At the initial phase of the test, the uniformly stretched hybrid fibers exhibited some localized weak points where first fiber breakage occurred. Each failure event seemed to allow unraveling of the fibers and facilitated increased elongation (Fig. 3A). Continuous elongation of the fibers resulted in progressive thinning of the parallely realigned fibers until final sample breakage was induced by sequential failure of individual fibers. The presence of multiple fracture events, also evident in stepped stress–strain curve, further reinforced this sequential fiber fracture mode (Fig. 3B). In addition, the stress–strain curve revealed a brittle-to-ductile transition during fracture of hybrid fibers. Consequently, two coordinated failure mechanisms could be derived, one by the blend fibers and another one by the pure gelatin fibers. In detail, upon tensile loading, the thin gelatin fibers within the hybrid assembly underwent brittle failure at low strains after
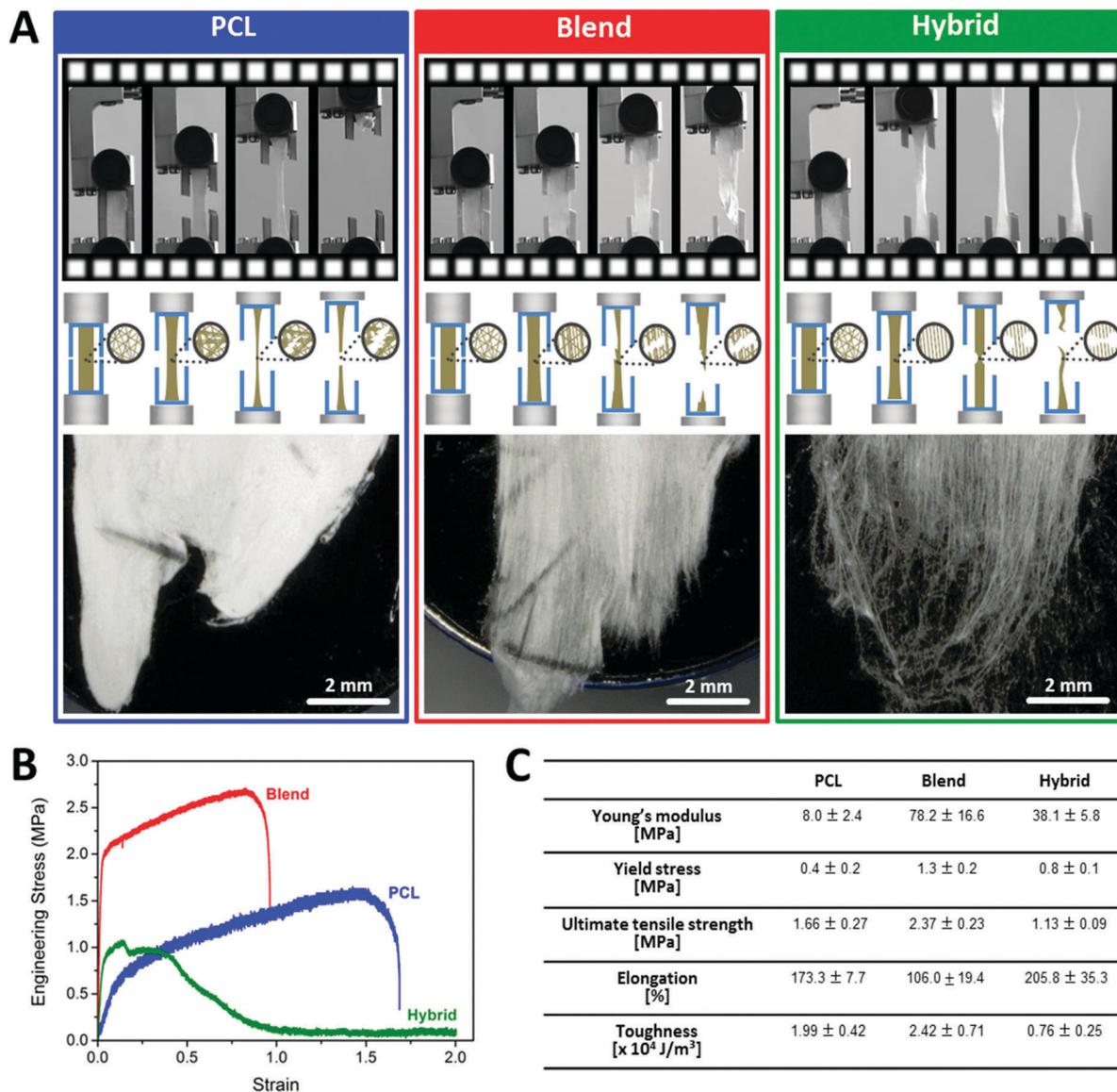
Fig. 3 Mechanical properties of electrospun PCL, blend and hybrid fiber mats. (A) Visualization of the different failure modes based on acquired time-lapsed serial images upon tensile loading and representative optical micrographs of the fracture fiber surfaces after mechanical testing. (B) Typical engineering stress–strain curves for each type of fiber mats. (C) Mechanical parameters calculated from the engineering stress–strain curves.

energy absorbance. Consequently, the load was transferred to the larger blend fibers, thereby providing more space for reorganization and alignment until final fiber fracture was attained in a ductile manner. Accordingly, the failure behavior of the hybrid fibers excellently correlated to the anisotropic mechanical behavior found in native ECM as described above.[18,19,22] High-speed video sequences of typical tensile loading tests for the different fibers are provided as ESI,† V1–V3. A detailed characterization of the fiber mechanics focusing on Young's modulus, toughness and elongation obtained from stress–strain curve calculations is summarized in Fig. 3C. In terms of elongation, all fibers could be stretched at least 100% of their original length before failure, with the highest elongation capability for hybrid fibers. As previously reported for collagen-rich tissue, extensive fiber deformation capability is of major importance for optimal biological function by minimizing brittle-like failure events.[20]

These findings highlight that effective modulation of biomechanical fiber properties can be governed by both, mechanical properties of the materials (brittle or ductile) and structural organization of different materials within the fiber matrix.

3.3 Degradation kinetics of gelatin from bio-adaptive hybrid fibers

In addition to the biomechanical properties, the surface properties of the fibers and the porosity of the mats play important roles for cell behavior as already mentioned above.[9,10,28,29] The hybrid fibers consist of gelatin as water-soluble polymer with good wettability and PCL which is not water-soluble and less wettable. The intention of mixing pure gelatin fibers with blend

fibers (PCL/gelatin) was to provide a dense fiber network for the initial phase of cell attachment with gelatin providing binding sites at the pure fibers as well as on the surface of the blend fibers. Upon slow degradation of the gelatin, the porosity of the fiber mat increases leaving more space for cell infiltration and migration into the remaining part of the blend fibers. To determine the degradation kinetics of gelatin within the hybrid scaffolds, we performed degradation studies in PBS buffer solution at 37 °C for a duration of four months. A combination of electron microscopy and confocal Raman microscopy was utilized to visualize changes during gelatin degradation. Before degradation, two fiber types with different diameters were identified within the hybrid fiber mats, the thinner ones being gelatin and the thicker ones being blend fibers (Fig. 4A). During the study, pure gelatin fibers were completely degraded, indicated by the absence of thin fibers on SEM micrographs, which could be confirmed by CRM examination (Fig. 4B). At a higher magnification, the degradation of gelatin can also be traced on the surface of the blend fibers. Before contact with liquid media, the fibers exhibit a smooth surface mainly based on gelatin (Fig. 4C). Upon degradation, the dissolved gelatin leaves small voids in the surface
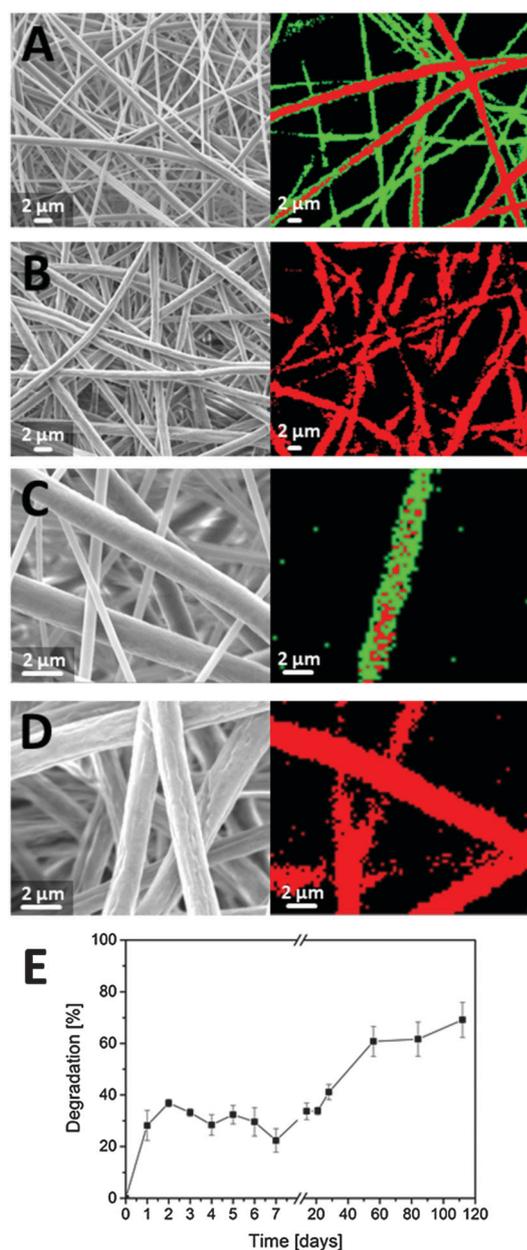

Fig. 4 Evaluation of degradation kinetics of gelatin from hybrid fiber mats using SEM and Raman analysis (PCL – red, gelatin – green); (A) before degradation; (B) after degradation; (C) before degradation at higher magnification exhibiting a smooth surface; (D) after degradation at higher magnification exhibiting a structured surface; (E) degradation kinetics of gelatin over four months.
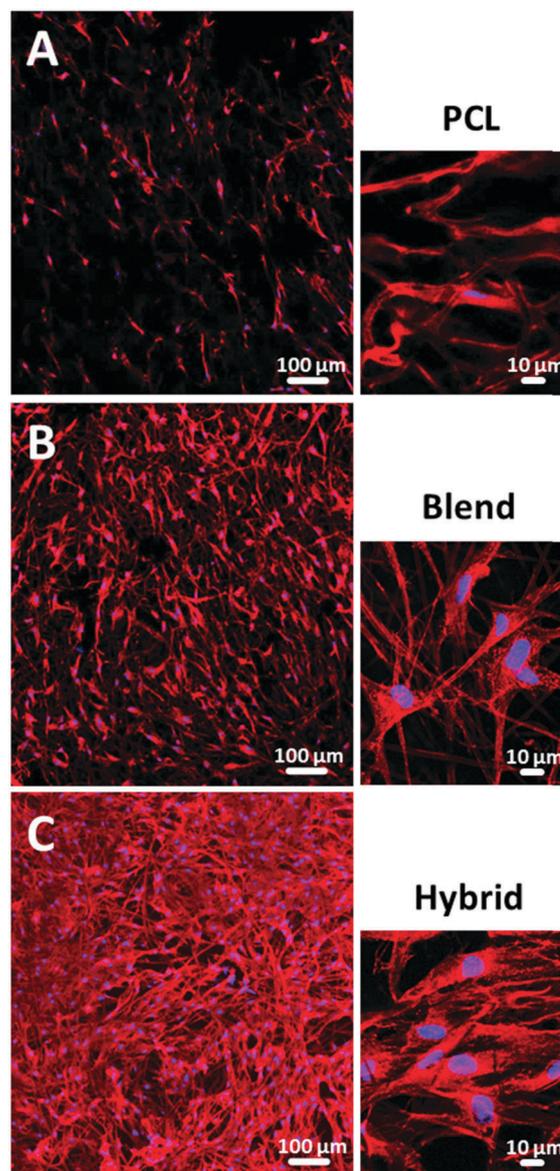

Fig. 5 Evaluation of cell–matrix interactions by analysis of cell behavior as response to fiber surface. Fluorescence staining of cell membrane (red) and cell nuclei (blue) to visualize human dermal fibroblasts cultivated for 14 days onto (A) PCL, (B) blend and (C) hybrid fiber mats revealing considerable differences in cell density and three-dimensional cell-shaping among these three electrospun fiber mats.

of the fibers visualized by electron microscopy in Fig. 4D. Such increase of "surface roughness" due to a soluble compound in blend fibers has already been reported by Xue et al.[33] Further, the degradation kinetics ideally match the requirements for the different phases of cell cultivation, providing a dense gelatin-rich structure in the first 24–48 hours for cell attachment. Subsequently, higher porosity due to degradation of the pure gelatin fibers facilitates cell infiltration and migration (Fig. 4E).

3.4 Assessment of cell–matrix interactions

As a next step, we cultivated primary human skin fibroblasts on all three fiber mats (pure PCL, blend and hybrid fibers) to analyze cell–fiber interactions for evaluating the suitability of each fiber mat type and elucidating critical composite attributes for imitation of native ECM. Among the three fabricated types of fibers, we observed considerable differences in terms of cell morphology and density. The level of cell coverage on the PCL fiber mats was rather low (Fig. 5A). This effect is due to the hydrophobic surface characteristics (contact angle 119°), which hamper optimal cell attachment as well as to low stiffness properties (8.0 MPa $\pm$ 2.5 MPa, n = 6) and moderate toughness (1.99 $\times$ 10^4 J m^{-3} $\pm$ 0.42, n = 6). In contrast, fiber mats consisting of a PCL/gelatin blend showed a higher cell density

and three-dimensional cell shaping induced by improved cell attachment properties due to the increased fiber hydrophilicity (contact angle 0°) as well as a considerable increase in stiffness (78.2 MPa $\pm$ 16.6 MPa, n = 6) and toughness (2.42 $\times$ 10^4 J m^{-3} $\pm$ 0.71, n = 6) (Fig. 5B). The highest level of cell growth and three-dimensional cell organization was visualized for the PCL/gelatin hybrid fiber mats. The cells were able to attach to multiple fibers due to their improved surface hydrophilicity and smaller pore sizes in the initial phase (Fig. 5C). To verify our findings regarding the supportive effect of hybrid fibers on cell proliferation based on qualitative analysis using fluorescence imaging in comparison to pure PCL and blend fibers, we further performed quantitative cell counting experiments. The data are presented as ESI,† S1.

The biodegradation of gelatin over time induced the fiber mat pore structure to dynamically change during cultivation allowing the cells to infiltrate the hybrid fiber mat as shown for human dermal fibroblasts (Fig. 6A) and human keratinocytes (Fig. 6B) based on z-stack analysis. These findings highlight the potential of the hybrid fiber mats as a suitable biomimetic structure comparable to native ECM.

3.5 Evaluation of hierarchical three-dimensional cultivation of human cells

Further, we evaluated the potential of the hybrid fiber mats for the hierarchical three-dimensional co-cultivation of different human skin cells. As previously reported, conventional two-dimensional culture surfaces significantly influence cell morphology and function e.g. flattening.[48–50] Three-dimensional cell cultures are generally grown with the use of hydrogel substrates.[51–54] However, obviously a gel is not mimicking the fiber structure and mechanical properties of native ECM.[55,56] In this study, we cultivated fibroblasts (as cells forming the dermis in human skin) on the fiber mats in a multi-well plate assembly equipped with permeable membrane inserts. After 14 days of cultivation, keratinocytes were seeded on top of this assembly to form the
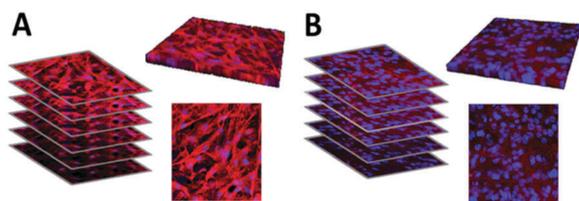

Fig. 6 Z-stack analysis of human-derived skin cells with fluorescence-staining of the cell membrane (red) and cell nuclei (blue) to visualize three-dimensional arrangement within electrospun hybrid fiber mats of (A) human dermal fibroblasts after 14 days of cultivation and (B) human keratinocytes after 10 days of submersed cultivation.
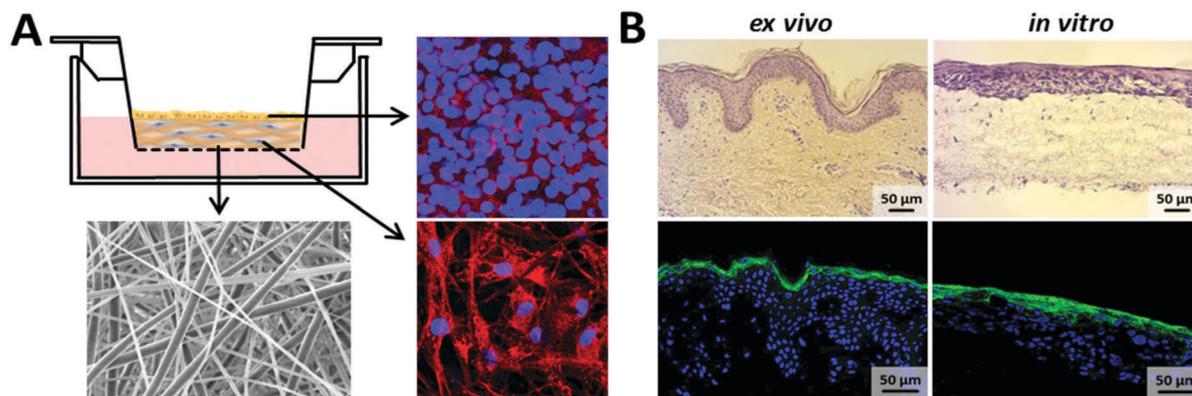

Fig. 7 Evaluation of the applicability of electrospun hybrid fiber mats for hierarchical co-cultivation of human-derived skin cells. (A) Experimental setup for in vitro reconstruction of human skin tissue using a Transwell®-system by first seeding human primary dermal fibroblasts on electrospun hybrid fiber mats for 14 days, followed by co-cultivation with human keratinocytes on top of the fiber mats surface for 10 days under submersed culture conditions and further cultivation at air–liquid interface for 14 days. (B) Example of in vitro reconstructed skin tissue visualized by hematoxylin/eosin staining and evaluation of barrier formation by immunofluorescence-staining of terminal differentiated keratinocytes (green) using involucrin (right column) compared to ex vivo human skin tissue (left column).

upper epidermal part of human skin. Subsequently, the inserts of the well plate were lifted to the air–liquid interface to induce a stratification of the upper keratinocyte layers,[57,58] thus mimicking the *in vivo* situation in the human body as illustrated in the schematic diagram of Fig. 7A. Representative fluorescence-based images of fibroblasts (bottom right corner) and keratinocytes (top right corner) cultivated on hybrid fibers are shown in Fig. 7A. Visualization of cell compartments was performed by fluorescence-based staining of the cell membrane (red) and cell nuclei (blue). The fibroblasts revealed a three-dimensional cellular organization in response to the hybrid fiber mat surface after two weeks of cultivation. The high cell density of keratinocytes detected on the hybrid fiber mat surface after ten days of submersed cultivation further reinforced the applicability of these hybrid fibers offering optimal conditions for cell growth. As the final step of our study, we compared the fiber mats with excised human skin by histological analysis based on cross sections stained with hematoxylin/eosin (Fig. 7B). Hematoxylin (blue) binds to cell nuclei, whereas eosin staining (pink) visualizes collagenous structures as the main constituents of the dermis part. As the direct comparison of fiber mat and excised human skin shows, a multilayered sheet of keratinocytes was evident and highly comparable to native epidermal structures. The presence and in-growth of the fibroblasts into the scaffold could clearly be visualized by the distribution of the fibroblast nuclei throughout the entire scaffold (Fig. 7B). Further, we verified the barrier formation by involucrin (green) as a specific immunofluorescence-based marker for terminal differentiation of the keratinocytes.[59,60] In addition, we used DAPI staining (blue) to visualize the cell nuclei, which are present in high density in the viable epidermis to confirm the corresponding localization of involucrin occurring towards the air exposed region above the viable part of the epidermis. A uniform consistent stratified layer was apparent as shown at the bottom right corner of Fig. 7B, indicating the presence of an intact barrier in our reconstructed skin along the entire length of the cross section with morphological similarity to the situation in the human body as visualized at the bottom left corner of Fig. 7B.

4. Conclusions

In summary, we fabricated biocompatible hybrid fibers simulating the complex biomechanical characteristics of native ECM in human skin. These three-dimensional fibrillar networks provide a unique bio-adaptive environment for cell attachment, migration, and proliferation within the fiber matrix without the necessity to attach additional growth factors. In interactions studies with skin cells, we demonstrated the mediating effect of tailored biomechanics, in combination with wettability and biodegradation of the fibers on cellular behavior, thus verifying the synergistic role of these key parameters to facilitate cell attachment and proliferation. Co-cultivation of fibroblasts and keratinocytes on the fiber mats resulted in a hierarchical organization of dermal and epidermal tissue layers with terminal cell differentiation. These findings provide valuable new insights into cell behavior

in three-dimensional structures and cell–material interactions which can be used for rational development of bio-inspired functional materials for advanced biomedical applications. Future studies will aim on a quantitative understanding of how local fiber properties determine the behavior on a three-dimensional tissue level.

Acknowledgements

References

1 Y. Bar-Cohen, *Bioinspiration Biomimetics*, 2006, **1**, P1.
2 N. F. Lepora, P. Verschure and T. J. Prescott, *Bioinspiration Biomimetics*, 2013, **8**, 013001.
3 C. Frantz, K. M. Stewart and V. M. Weaver, *J. Cell Sci.*, 2010, **123**, 4195.
4 O. Guillame-Gentil, O. Semenov, A. S. Roca, T. Groth, R. Zahn, J. Vörös and M. Zenobi-Wong, *Adv. Mater.*, 2010, **22**, 5443.
5 R. Xu, M. B. Taskin, M. Rubert, D. Seliktar, F. Besenbacher and M. Chen, *Sci. Rep.*, 2015, **5**, 8480.
6 T. C. Reis, S. Castleberry, A. M. Rego, A. Aquiar-Ricardo and P. T. Hammond, *Biomater. Sci.*, 2016, **4**, 319.
7 M. Norouzi, S. M. Boroujeni, N. Omidvarkordshouli and M. Soleimani, *Adv. Healthcare Mater.*, 2015, **4**, 1114.
8 S. Drotleff, U. Lungwitz, M. Breunig, A. Dennis, T. Blunk, J. Tessmar and A. Göpferich, *Eur. J. Pharm. Biopharm.*, 2004, **58**, 385.
9 N. M. Alves, I. Pashkuleva, R. L. Reis and J. F. Mano, *Small*, 2010, **6**, 2208.
10 J. Pelipenko, P. Kocbek, B. Govedarica, R. Rošic, S. Baumgartner and J. Kristl, *Eur. J. Pharm. Biopharm.*, 2013, **84**, 401.
11 H. Rashidi, J. Yang and K. M. Shakesheff, *Biomater. Sci.*, 2014, **2**, 1318.
12 S. W. Cranford, J. de Boer, C. van Blitterswijk and M. J. Buehler, *Adv. Mater.*, 2013, **25**, 802.
13 S. Cranford and M. J. Buehler, *Nanotechnol., Sci. Appl.*, 2010, **3**, 127.
14 M. J. Buehler, *MRS Bull.*, 2013, **38**, 169.
15 L. D. Muiznieks and F. W. Keeley, *Biochim. Biophys. Acta*, 2013, **1832**, 866.
16 N. Naik, J. Caves, E. L. Chaikof and M. G. Allen, *Adv. Healthcare Mater.*, 2014, **3**, 367.
17 Z. Zhang and B. B. Michniak-Kohn, *Pharmaceutics*, 2012, **4**, 26.
18 A. Ní Annaidh, K. Bruyère, M. Destrade, M. D. Gilchrist and M. Otténio, *J. Mech. Behav. Biomed. Mater.*, 2012, **5**, 139.
19 R. H. Pritchard, Y. Y. Huang and E. M. Terentjev, *Soft Matter*, 2014, **10**, 1864.
20 M. J. Buehler, *Proc. Natl. Acad. Sci. U. S. A.*, 2006, **103**, 12285.
21 A. Gautieri, S. Vesentini, A. Redaelli and M. J. Buehler, *Nano Lett.*, 2011, **11**, 757.

22 Y. Tang, R. Ballarini, M. J. Buehler and S. J. Eppell, *J. R. Soc., Interface*, 2010, **7**, 839.

23 P. Boukamp, R. T. Petrussevska, D. Breitkreutz, J. Hornung, A. Markham and N. E. Fusenig, *J. Cell Biol.*, 1988, **106**, 761.

24 N. Oliva, S. Unterman, Y. Zhang, J. Conde, H. S. Song and N. Artzi, *Adv. Healthcare Mater.*, 2015, **4**, 1584.

25 T. Sun, D. Norton, R. J. McKean, J. W. Haycock, A. J. Ryan and S. MacNeil, *Biotechnol. Bioeng.*, 2007, **97**, 1318.

26 J. L. Lowery, N. Datta and G. C. Rutledge, *Biomaterials*, 2010, **31**, 491.

27 J. Pelipenko, P. Kocbek and J. Kristl, *Eur. J. Pharm. Sci.*, 2014, **66C**, 29.

28 M. Nikkhah, F. Edalat, S. Manoucherie and A. Khademhosseini, *Biomaterials*, 2012, **33**, 5230.

29 W. Zheng, W. Zhang and X. Jiang, *Adv. Healthcare Mater.*, 2013, **2**, 95.

30 M. A. Woodruff and D. W. Hutmacher, *Prog. Polym. Sci.*, 2010, **35**, 1217.

31 Z.-M. Huang, Y. Z. Zhang, S. Ramakrishna and C. T. Lim, *Polymer*, 2004, **45**, 5361.

32 Y. Zhang, H. Ouyang, C. T. Lim, S. Ramakrishna and Z.-M. Huang, *J. Biomed. Mater. Res., Part B*, 2005, **72**, 156.

33 J. Xue, M. He, H. Liu, Y. Niu, A. Crawford, P. D. Coates, D. Chen, R. Shi and L. Zhang, *Biomaterials*, 2014, **35**, 9395.

34 S. Gautam, A. K. Dinda and N. C. Mishra, *Mater. Sci. Eng., C*, 2013, **33**, 1228.

35 L. Ghasemi-Mobarakeh, M. P. Prabhakaran, M. Morshed, M. H. Nasr-Esfahani and S. Ramakrishna, *Biomaterials*, 2008, **29**, 4532.

36 E. J. Chong, T. T. Phan, I. J. Lim, Y. Z. Zhang, B. H. Bay, S. Ramakrishna and C. T. Lim, *Acta Biomater.*, 2007, **3**, 321.

37 P. T. Hwang, K. Murdock, G. C. Alexander, A. D. Salaam, J. I. Ng, D. J. Lim, D. Dean and H. W. Jun, *J. Biomed. Mater. Res., Part A*, 2016, **104**, 1017.

38 S. Gautam, C. F. Chou, A. K. Dinda, P. D. Potdar and N. C. Mishra, *Mater. Sci. Eng., C*, 2014, **34**, 402.

39 D. E. Discher, P. Janmey and Y.-L. Wang, *Science*, 2005, **310**, 1139.

40 R. G. Wells, *Hepatology*, 2008, **47**, 1394.

41 B. Geiger, J. P. Spatz and A. D. Bershadsky, *Nat. Rev. Mol. Cell Biol.*, 2009, **10**, 21.

42 S. Wong, W.-H. Guo and Y.-L. Wang, *Proc. Natl. Acad. Sci. U. S. A.*, 2014, **111**, 17176.

43 C. T. Koh and M. L. Oyen, *J. Mech. Behav. Biomed. Mater.*, 2012, **12**, 74.

44 R. O. Ritchie, *Nat. Mater.*, 2011, **10**, 817.

45 M. E. Launey and R. O. Ritchie, *Adv. Mater.*, 2009, **21**, 2103.

46 C. T. Koh, D. G. Strange, K. Tonsomboon and M. L. Oyen, *Acta Biomater.*, 2013, **9**, 7326.

47 U. G. Wegst, H. Bai, E. Saiz, A. P. Tomsia and R. O. Ritchie, *Nat. Mater.*, 2015, **14**, 23.

48 F. Pampaloni, E. G. Reynaud and E. H. K. Stelzer, *Nat. Rev. Mol. Cell Biol.*, 2007, **8**, 839.

49 H. Page, P. Flood and E. G. Reynaud, *Cell Tissue Res.*, 2013, **352**, 123.

50 E. Knight and S. Przyborski, *J. Anat.*, 2015, **227**, 746.

51 T. Elsdale and J. Bard, *Cell Biol.*, 1972, **54**, 626.

52 E. Bell, H. P. Ehrlich, D. J. Buttle and T. Nakatsuji, *Science*, 1981, **211**, 1052.

53 R. A. Brown, *Exp. Cell Res.*, 2013, **319**, 2460.

54 R. Dong, Y. Pang, Y. Su and X. Zhu, *Biomater. Sci.*, 2015, **3**, 937.

55 H.-J. Stark, M. J. Willhauck, N. Mirancea, K. Boehnke, I. Nord, D. Breitkreutz, A. Pavesio, P. Boukamp and N. E. Fusenig, *Eur. J. Cell Biol.*, 2004, **83**, 631.

56 M. L. Oyen, *Int. Mater. Rev.*, 2014, **59**, 44.

57 M. Fartasch and M. Ponec, *J. Invest. Dermatol.*, 1994, **102**, 366.

58 M. O. Danso, T. Berkers, A. Mieremet, F. Hausil and J. A. Bouwstra, *Exp. Dermatol.*, 2015, **24**, 48.

59 F. M. Watt, *J. Invest. Dermatol.*, 1983, **81**, 100s.

60 E. Candi, R. Schmidt and G. Melino, *Nat. Rev. Mol. Cell Biol.*, 2005, **6**, 328.